

An Idealized Study of the Structure of Long, Partially Mixed Estuaries*

ROBERT D. HETLAND

Department of Oceanography, Texas A&M University, College Station, Texas

W. ROCKWELL GEYER

Woods Hole Oceanographic Institution, Woods Hole, Massachusetts

(Manuscript received 17 February 2004, in final form 1 June 2004)

ABSTRACT

Classic models of estuarine circulation are reexamined using a three-dimensional, primitive equation numerical ocean model. The model is configured using an idealized estuary/shelf domain with rectangular cross section, constant vertical mixing, and steady riverine discharge. Tidal dispersion is neglected, so the analysis does apply to well-mixed estuaries and lagoons. Estuarine scales for the length of steady-state salt intrusion, vertical stratification, and estuarine exchange flow estimated from steady-state model results are found to have the same functional relationships to vertical mixing and riverine discharge as the classic analytic solutions. For example, for steady-state conditions, the stratification is found to be virtually independent of the strength of vertical mixing. The estuarine structure was controlled by the interior estuarine circulation, and not by limited exchange at the mouth. Thus, the numerical solutions were not "overmixed," although the solutions showed a dependence on freshwater flux functionally similar to the overmixed solution. Estuarine adjustment time scales are also estimated from the simulations, and they are related to the steady-state estuarine scales. Two classes of nonsteady solutions are examined: the response to a step change in riverine discharge and estuarine response to changes in vertical mixing. Spring/neap tidal variations are examined by modulating the (spatially constant) vertical mixing with a fortnightly period. Unlike the steady solutions, there is a clear dependence of stratification on mixing rate in the time-dependent solutions. The simulations involving changes in riverine discharge show asymmetries between response to increasing and decreasing river flow that are attributed to quadratic bottom drag.

1. Introduction

Over 50 years ago, Pritchard (1952) defined the basic dynamics of estuarine circulation and Hansen and Rattray (1965) followed with an analytical solution for the estuarine momentum and salt equations. These solutions formed the basis for an estuarine classification scheme (Hansen and Rattray 1966) that is still widely applied. However, the simplifications required to achieve the Hansen and Rattray solution limit the realism of the results; for example, the vertical mixing coefficients are assumed to be constant in time and space, and tidal advection is not considered. Yet, this solution embodies the essential elements of the estuarine exchange flow, and there are still aspects of the solution that are not fully appreciated.

For example, in estuaries in which the estuarine ex-

change flow dominates the longitudinal salt flux, the steady solutions of Hansen and Rattray (1965) and Chatwin (1976) have the peculiar characteristic that neither the shear nor the stratification depends on the vertical mixing rate. This result contradicts the common observation of spring–neap variability in estuarine stratification and exchange flow, which is explained by variations in vertical mixing rate (Hass 1977; Jay and Smith 1990; Linden and Simpson 1988). As noted by MacCready (1999), this apparent discrepancy between the analytical solution and observations is due to the time-dependent adjustment of the estuary to changes in forcing, where the time scale of adjustment of the stratification and shear to a change in mixing is generally much faster than the response of the horizontal salinity gradient. Thus, the observed spring–neap variations in stratification and exchange flow is a fundamentally time-dependent response, inconsistent with the idealized, steady solution for estuarine exchange flow.

This paper reports on a numerical study of an idealized estuary, focusing on the longitudinal and vertical structure of salinity and velocity as they vary with changes in freshwater inflow and vertical mixing rate.

* Woods Hole Oceanographic Institution Contribution Number 11166.

Corresponding author address: Dr. Robert Hetland, Department of Oceanography, Texas A&M University, College Station, TX 77843.
E-mail: hetland@tamu.edu

The estuarine domain is “narrow” in the sense that it does not include rotation or lateral depth variations that would induce lateral variations in circulation. The domain is also “long” in the sense that the salinity intrusion length is always controlled by the estuarine dynamics rather than the physical length of the basin. The approach follows from the analytical formulations of Pritchard (1952, 1954), Hansen and Rattray (1965), and Chatwin (1976), in that the geometry is idealized and the mixing is constant throughout the estuary, but relaxes certain assumptions required by the analytical solutions, such as a linearized momentum balance. The numerical approach also allows the examination of time-dependent solutions, relevant to changes in freshwater flow and spring–neap changes in mixing. The modeling approach retains a number of simplifications relative to real estuaries, such as neglect of lateral variability, constant vertical mixing coefficient, and neglect of tidal processes (except insofar as they set the vertical mixing coefficient). Although these simplifications may limit the quantitative application of the results, they allow an examination of the essential nature of the response of the estuarine circulation to the two main forcing agents: the freshwater flow and the intensity of vertical mixing.

One of the broad goals of this paper is determine the scaling for the time scale of estuarine adjustment. We find, as others have, that it is possible to approximate the adjustment time scales in terms of the steady-state length and velocity scales (Kranenburg 1986; MacCready 1999). More subtle issues are also investigated, involving the details of the estuarine dynamics and adjustment processes. For instance, we find that there is an asymmetry in the response of the estuary to an increase or decrease in freshwater flux due to the nonlinear effects of bottom drag. In addition, although in some instances the exchange of an estuary with the ocean may be limited by the exchange flow at the estuary mouth (e.g., Stommel and Farmer 1953), in our numerical results the estuarine exchange is instead controlled by interior dynamics for the geometry and configuration that we have chosen. However, even in this case the exchange has the same functional dependence on freshwater flow as the Stommel and Farmer (1953) overmixing solution; the simulated exchange flow and stratification are consistently about 70% of the theoretical overmixed limits.

The numerical setup that we chose was inspired by estuaries like the Hudson and James, although direct comparisons between observations in these systems and numerical results would be inappropriate because of the many simplifying assumptions used in keeping with the spirit of an analytical solution. Most notable, tides are not included in the simulations, which eliminates the influence of tidal dispersion. In our simulations, the vertical structure of the estuary is well resolved, allowing a detailed examination of the partially mixed regime. MacCready (1999) addressed issues similar to those addressed in this paper using a two layer estuary model

in a limited domain; the numerical modeling approach is the fundamental difference between these two studies.

The remainder of the paper is structured as follows. Section 2 reviews previous analytical solutions for steady and time-dependent estuarine scales. Section 3 describes the numerical model. Section 4 presents the steady-state results of the numerical model for constant forcing conditions. Section 5 explores the time-dependent behavior of the system related to temporal changes in freshwater flow and mixing rate. Section 6 compares the numerical solutions to Stommel and Farmer’s (1953) overmixed estuary solution. Sections 7 and 8 provide further discussion and conclusions.

2. Theory

The numerical results presented in this paper are compared to a variety of previously derived analytical models for steady-state estuarine structure, time scales of estuarine adjustment, and control conditions on exchange at the estuary mouth. These theories are reviewed, respectively, in the following three sections.

a. Steady-state scaling

In this paper, we follow the dynamical construct of Chatwin (1976): an estuary with uniform depth in which the longitudinal salt flux is steady and dominated by the horizontal exchange flow, and cross-channel variations are ignored. However, we later relax Chatwin’s assumption that the along-channel momentum equation is linearized. Chatwin’s expressions for estuarine velocity and stratification are

$$u_e = -\frac{\beta g H^3}{48 \nu} \left(\frac{\partial s}{\partial x} \right) f_1(z') + \frac{3}{2} u_f f_2(z') \quad \text{and} \quad (1)$$

$$\frac{\partial s}{\partial z} = -\frac{\beta g H^4}{48 \nu K_z} \left(\frac{\partial s}{\partial x} \right)^2 f_3(z') - \frac{u_f H}{K_z} \left(\frac{\partial s}{\partial x} \right) f_4(z'), \quad (2)$$

where β is the parameter relating salinity s to density ρ [i.e., $\rho = \rho_0(1 + \beta s)$], u_f is the depth average velocity, u_e is the vertical exchange flow (with a mean of zero, so $u = u_f + u_e$), g is the acceleration of gravity, H is the water depth, ν is the viscosity, K_z is the vertical diffusivity, and f_1 , f_2 , f_3 , and f_4 are nondimensional $O(1)$ polynomials in $z' = z/H$. The first term in Eq. (1) is the baroclinic forcing term; the second term is due to the direct contribution of the river flow. Chatwin’s analysis is based on the assumption that the river flow is small relative to the estuarine circulation, causing the first term to dominate. This assumption is valid in most estuarine environments, the exception being strongly forced salt-wedge regimes. It is also assumed that the horizontal salt gradient weakly depends on depth, which is also violated in salt wedges.

Equation (2), describing the vertical stratification, also has two terms representing the contribution of the

density-driven shear and that of the river-flow-induced shear to maintaining the stratification against the influence of vertical mixing. As in the momentum equation, the second term is small except in strongly forced regimes, which lie outside the range of Chatwin's analysis.

The third equation determining the estuarine circulation represents the balance between the export of salt by the mean flow and the import by the estuarine circulation. Using Eqs. (1) and (2) but neglecting the second term in each (i.e., assuming the estuarine exchange is much stronger than the mean flow), Chatwin obtained an expression for this balance as

$$u_f s_0 = \int u_e (s - s_0) dz = \left(\frac{19}{630 \times 48^2} \right) \frac{\beta^2 g^2 H^8}{\nu^2 K_z} \left(\frac{\partial s}{\partial x} \right)^3, \quad (3)$$

where s_0 is the vertically averaged salinity in the middle of the estuary. This equation indicates the relationship between the horizontal salinity gradient, the freshwater flow, and the vertical mixing rate, given a regime in which the salt flux is dominated by the estuarine circulation rather than other dispersive processes. One notable aspect of this solution that is not pursued further in this paper is the very sensitive dependence of the estuarine salt flux on depth. Chatwin's solution is very similar to the Hansen and Rattray (1965) solution in the limit of small longitudinal diffusion. This limit is relevant to partially mixed estuaries like the Hudson (Abood 1974; Hunkins 1981), and it is the case examined in this paper.

The variables of relevance to this paper are the freshwater flow and the vertical mixing rate. To simplify the consideration of vertical mixing, we will assume that viscosity is proportional to diffusivity, assuming the variable κ is proportional to both K_z and ν , for scaling purposes. Given this simplification, the horizontal salinity gradient is found to depend on the freshwater flow and mixing rate as

$$\frac{\partial s}{\partial x} = C_1 \kappa u_f^{1/3}, \quad (4)$$

where C_1 is a constant obtained from the other terms in Eq. (3). Note that the horizontal salinity gradient depends linearly on the vertical mixing rate—stronger mixing results in a stronger horizontal salinity gradient, that is, a shorter salinity intrusion. The gradient is much less sensitive to the freshwater inflow rate, as was pointed out by Hansen and Rattray (1965).

This scaling relation can then be substituted into the dominant terms in Eqs. (1) and (2) to obtain the scaling for estuarine velocity and stratification as

$$u_e = C_2 u_f^{1/3} \quad \text{and} \quad (5)$$

$$\frac{\partial s}{\partial z} = C_3 u_f^{2/3}, \quad (6)$$

where C_2 and C_3 are constants that depend on the other terms in Eqs. (1) and (2) and on the ratio of viscosity to diffusivity, that is, the turbulent Prandtl number ($\text{Pr} \equiv \nu/K_z$).

What is striking about this solution is that neither the estuarine velocity nor the stratification depends on the vertical mixing rate, even though the vertical mixing is a key part of both the momentum and salt balances. The reason for this is that the variations in mixing influence the magnitude of the horizontal salinity gradient in the correct proportion so as to cancel out its influence on the momentum and stratification equations. As vertical mixing becomes stronger, the horizontal estuarine salinity gradient gets stronger, leading to the same velocity and salinity structure for different mixing rates.

The numerical experiments presented in section 4 provide a test of the theory with the relaxation of some of the limiting assumptions required for an analytical result. The scaling is found to apply across a broad range of forcing conditions for the steady-state analysis.

b. Time-dependent response of an estuary

Kranenburg (1986) derives an analytical scaling for the adjustment time scale of a well-mixed estuary in which the freshwater flux has suddenly changed:

$$\tau_u = \frac{1}{s_0} \int_0^L A \left| \frac{\partial s}{\partial Q_f} \right| dx, \quad (7)$$

where A is the cross-sectional area of the estuary, Q_f is the freshwater transport, $s(x, Q_f)$ is the steady-state, cross-sectional average salinity given Q_f , and s_0 is the oceanic salinity at the estuary mouth. The time scale τ_u may also be estimated by dividing the ultimate change in freshwater content in the estuary by the change in freshwater flux.

The time scale of adjustment, τ_u , can be compared with the freshwater advective time scale $\tau_f = L/u_f$, the time it would take a particle traveling with the freshwater velocity u_f to traverse an estuary of length L . For a prismatic estuary, like those described by Hansen and Rattray (1965), Chatwin (1976), and this study, Kranenburg derives an adjustment time scale that is 1/6 as fast as the advective time scale. The adjustment time scale is much slower than the advective time scale because of the small exponent in Eq. (4). Because of this, we define a "speedup factor,"

$$\alpha_u = \tau_f / \tau_u. \quad (8)$$

Assuming a constant along-channel salinity gradient, geometric arguments may also be used to derive $\alpha_u = 6$. Kranenburg suggests, but does not show, that a similar adjustment time scale is appropriate for changes in vertical mixing.

MacCready (1999) reexamined the time-dependent response of estuaries to both mixing and changes in freshwater flux using a two-layer numerical model of

estuarine circulation. Qualitatively, his results agree with Kranenburg (1986), although his results are influenced by the limited domain (the estuarine length scale is longer than the length of the estuary channel). If the adjustment time scale of the two-layer model is recalculated with an estuary channel length that exceeds the length of the salt penetration so that the salt penetration is not bounded by topography, the adjustment time scale caused by a change in freshwater flux reduces to that calculated by Kranenburg (1986) (P. MacCready 2003, personal communication). MacCready points out that the tidal mixing case has two distinct time scales. First, there is the (typically) faster adjustment time scale of the horizontal exchange flow ($\Delta u \Delta s$), which comes to an equilibrium with the new vertical mixing on approximately the vertical mixing time scale [$O(H^2/\kappa)$ in the notation of this paper]. Second, there is the longer time scale of the adjustment of the longitudinal salt structure (L in the notation of this paper), which is relevant to the 1D analysis of Kranenburg. In all of the cases MacCready covered, as well as all the cases in this paper, the vertical mixing scale was quicker than the estuarine length scale adjustment time scale.

c. Overmixing theory

Conservation of mass and salt may be used to demonstrate how increased mixing will increase estuarine exchange. As the salinity of the outflow increases, so does the magnitude of the exchange flow. However, estuarine exchange will eventually be limited by hydraulic control at the estuary mouth so that increased mixing does not further increase estuarine exchange. Stommel and Farmer (1953) refer to this limit as “overmixed” and examine outflow properties for this maximal exchange by approximating the exchange as a two-layer flow.

In the absence of tides, an internal hydraulic control occurs at the estuary mouth. (Hydraulic control may also be important in the presence of tides, but those time-dependent dynamics are complex and are not considered here.) This hydraulic control puts an upper bound on the allowable exchange. Overmixing occurs when the exchange is limited by hydraulic control, rather than internal estuarine mixing (Stommel and Farmer 1953). The control condition is approximated for small density differences as

$$G^2 = \frac{u_1^2}{g'h_1} + \frac{u_2^2}{g'h_2} = Fr_1^2 + Fr_2^2 = 1, \quad (9)$$

where Fr_1 and Fr_2 are the respective upper and lower layer Froude numbers and G is the composite Froude number (Armi and Farmer 1986; Stommel and Farmer 1953). The upper-layer transport, $u_1 h_1$, is always greater, since the upper layer carries the river discharge in addition to the exchange flow. For submaximal conditions ($h_1 < h_2$), the lower layer only makes a minor contribution to the composite Froude number. As the ex-

change flow increases, the interface depth must increase. Eventually, the interface cannot get any deeper because the lower layer starts making an appreciable contribution to the composite Froude number. The limiting case, at which the exchange flow is maximal, occurs with the interface somewhat deeper than middepth (for a rectangular cross section). For larger freshwater flows the interface is much deeper than middepth, and for weak freshwater flows, it is close to middepth.

Using Eq. (9) and imposing mass and salt balances, Stommel and Farmer (1953) estimate the upper-layer thickness for maximal exchange. From this, it is straightforward to calculate stratification and exchange flow at the mouth. In this paper, numerical solutions are compared with these values to determine whether the mixing in the estuary, associated with the exchange flow at the mouth, can become strong enough to reach the overmixing limit.

Because in Stommel and Farmer’s overmixing theory, the estuarine exchange is controlled at the mouth as opposed to internal estuarine dynamics, stratification and exchange flow are functions of river discharge alone. This dependence is functionally identical to Chatwin’s (1976) theory in that the stratification depends on $u_f^{2/3}$ and exchange flow on $u_f^{1/3}$ [see Eqs. (5) and (6)]. In both solutions, vertical mixing does not affect stratification or exchange flow; however, the Chatwin solution does depend on the Prandtl number. In the limit where exchange is large and the freshwater Froude number ($u_f^2/g\beta s_2 H$) is small, the two solutions are equivalent for $Pr = 630/(19 \times 32 \times 48) = 0.0216$. This small value is not likely to occur in nature, and so the exchange in a rectangular estuary would likely be limited by the estuarine dynamics rather than hydraulic control. This issue is explored in the numerical experiments that follow.

3. Numerical model description

The Regional Ocean Modeling System (ROMS; Haidvogel et al. 2000) was configured for the domain shown in Fig. 1. ROMS is a free-surface, hydrostatic, primitive equation ocean model that uses a stretched terrain-following coordinate in the vertical. At the “river” end of the estuary a freshwater transport of Q_f is specified. The volume transport introduces water with specified water properties into the domain; the inflowing river water is specified to have a salinity of zero and temperature of 4°C, identical to the background temperature set throughout the entire domain. The estuary is 1 km across and 10 m deep. The cross-sectional area of the domain is uniform (10^4 m^2), except for slight variations in the free surface, so that the volume transport may be converted into a freshwater velocity, u_f .

In the coastal ocean, a weak flow (0.05 m s^{-1}) directed in the sense of Kelvin wave propagation is set to prevent the formation of a bulge of freshwater at the estuary mouth (e.g., Yankovsky and Chapman 1997;

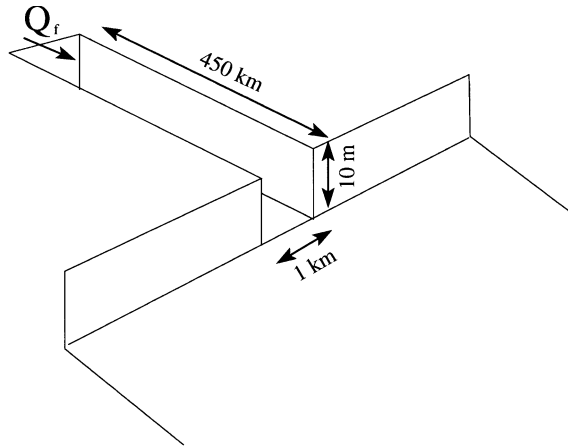


FIG. 1. The model domain used in the numerical simulations includes a rectangular channel attached to a shallow coastal ocean.

Fong 1998; Nof and Pichevin 2001), which could potentially choke the estuarine inflow. This background coastal flow also helps to maintain a constant salinity (32 psu) for the coastal oceanic water entering the estuary. Diffusivity and viscosity are set to the same constant value, κ , throughout the domain (i.e., a Prandtl number of 1), for a direct comparison with the analytical results shown in the previous section. The coastal ocean is explicitly included in the present domain despite the

increased computational expense required for the larger grid because we find it important that the internal hydraulic control condition (Armi and Farmer 1986) at the estuary mouth was unaffected by contamination from boundary conditions.

The discretized domain consists of a grid $59 \times 19 \times 10$, with the estuary resolved by 50 grid cells along the channel ($\Delta x \sim 3$ km) and 7 grid cells across the channel ($\Delta y \sim 142$ m). In the estuary, the vertical resolution is 1 m. The grid is “telescoped” near the river end; the along-channel resolution is gradually increased to $\Delta x \sim 42$ km, and so the channel can be longer without increasing the computational expense. The total length of the channel is 450 km, with the 140-km section adjacent to the ocean well resolved. Bottom friction is parameterized using a quadratic drag law.

4. Steady-state results

The model was run to steady state for a number of different values of diffusivity/viscosity and riverine discharge, ranging from $\kappa = 5.0 \times 10^{-5}$ to $1.0 \times 10^{-3} \text{ m}^2 \text{ s}^{-1}$, and $u_f = 0.01\text{--}0.3 \text{ m s}^{-1}$ (see Table 1). Note that tides are not explicitly modeled, as mentioned in section 2. However, the influence of time-dependent tidal mixing is parameterized through κ so that stronger tides are associated with higher mixing.

A diagram showing the steady state, along-channel

TABLE 1. Estuarine properties (length scale, circulation, stratification, and local Froude number) given as a function of the forcing (u_f and κ). Subscripts 1 and 2 represent values in the upper and lower layers, respectively. Scales were calculated by methods described in the appendix. The Froude numbers (Fr_1 , Fr_2 , and G) are defined in the section 2.

u_f (m s^{-1})	$\kappa (\times 10^4)$ ($\text{m}^2 \text{ s}^{-1}$)	τ_f (days)	L (km)	u_1 (m s^{-1})	u_2 (m s^{-1})	Δu (m s^{-1})	S_1 (psu)	S_2 (psu)	ΔS (psu)	Fr_1	Fr_2	G
0.01	0.5	546	472	0.14	-0.09	0.23	20.7	24.6	3.8	0.41	0.21	0.46
0.01	1.0	262	226	0.14	-0.09	0.23	20.5	24.3	3.7	0.41	0.23	0.46
0.01	2.0	147	127	0.14	-0.10	0.24	21.1	24.8	3.7	0.41	0.24	0.47
0.01	5.0	67	58	0.14	-0.10	0.24	21.7	25.3	3.5	0.41	0.27	0.49
0.01	10.0	37	32	0.14	-0.11	0.25	21.5	24.9	3.3	0.41	0.30	0.51
0.02	0.5	181	313	0.18	-0.10	0.28	18.3	24.1	5.7	0.41	0.20	0.46
0.02	1.0	107	185	0.18	-0.11	0.28	18.5	24.1	5.6	0.41	0.22	0.47
0.02	2.0	57	99	0.18	-0.11	0.29	18.8	24.4	5.5	0.41	0.24	0.47
0.02	5.0	25	44	0.18	-0.12	0.29	18.3	23.5	5.1	0.41	0.26	0.49
0.02	10.0	13	24	0.18	-0.12	0.30	18.1	23.0	4.9	0.42	0.29	0.50
0.05	0.5	53	231	0.25	-0.12	0.37	14.0	23.8	9.7	0.43	0.19	0.47
0.05	1.0	30	130	0.25	-0.13	0.37	14.0	23.4	9.4	0.43	0.21	0.47
0.05	2.0	16	70	0.25	-0.13	0.38	14.5	23.8	9.2	0.43	0.22	0.48
0.05	5.0	7	30	0.24	-0.14	0.39	14.3	23.2	8.8	0.42	0.24	0.49
0.05	10.0	3	15	0.25	-0.15	0.40	15.3	24.0	8.7	0.43	0.27	0.51
0.10	0.5	20	176	0.32	-0.13	0.45	9.4	23.0	13.6	0.45	0.18	0.49
0.10	1.0	11	97	0.32	-0.14	0.46	10.5	24.0	13.5	0.45	0.20	0.49
0.10	2.0	6	52	0.32	-0.15	0.47	10.7	24.0	13.3	0.45	0.21	0.50
0.10	5.0	3	23	0.32	-0.16	0.48	11.0	23.9	12.9	0.45	0.23	0.50
0.10	10.0	1	11	0.32	-0.16	0.48	10.1	21.9	11.7	0.45	0.25	0.52
0.30	0.5	3	83	0.50	-0.12	0.62	3.5	22.8	19.3	0.53	0.16	0.55
0.30	1.0	2	42	0.52	-0.14	0.65	4.1	24.5	20.5	0.53	0.18	0.56
0.30	2.0	1	23	0.51	-0.14	0.65	4.0	24.1	20.0	0.53	0.18	0.56
0.30	5.0	0.4	10	0.52	-0.15	0.67	4.1	23.8	19.6	0.53	0.21	0.57
0.30	10.0	0.2	6	0.56	-0.17	0.73	4.0	25.0	21.0	0.57	0.22	0.61

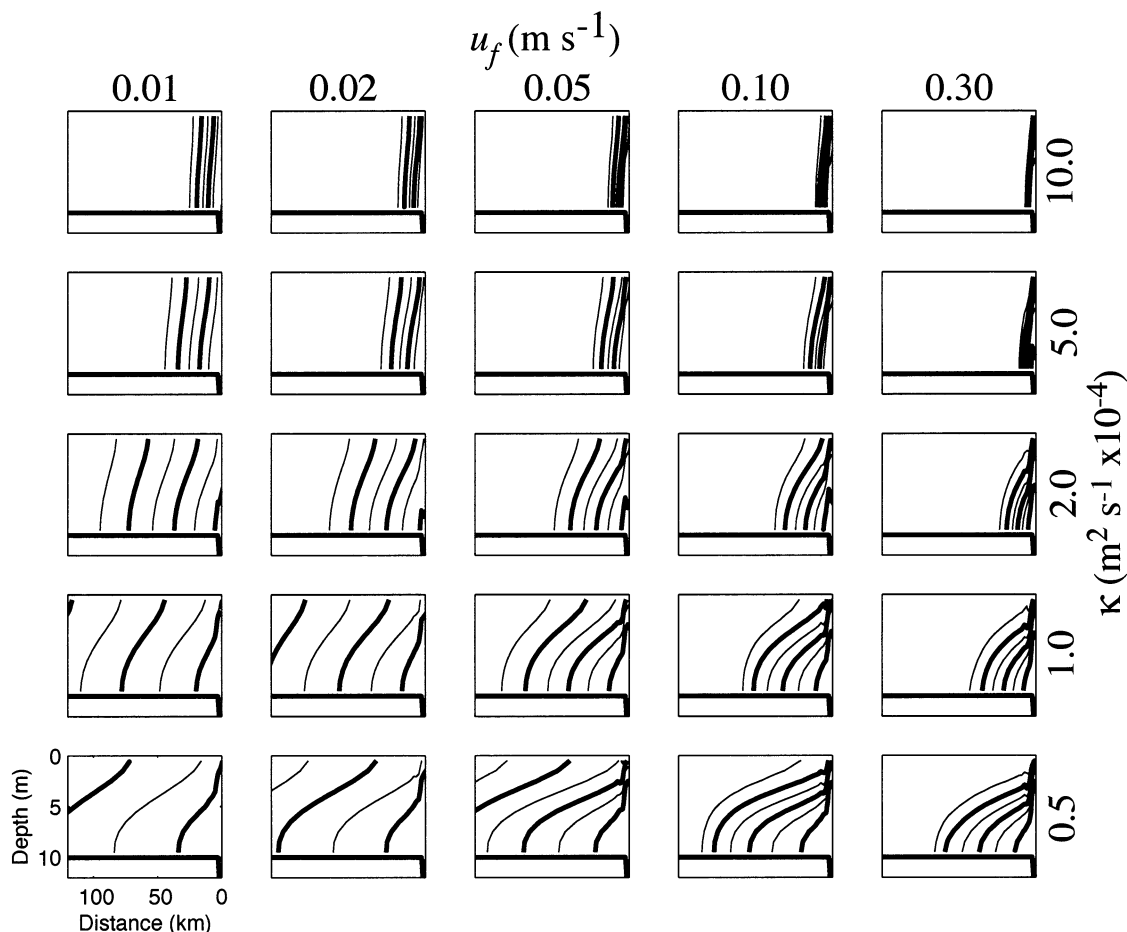


FIG. 2. Along-channel salt structure across parameter space. The figures show contours of salinity along the center of the channel, with thick contours every 10 psu, and thin contours at the intermediate +5 psu isohalines.

estuarine salt structure over this parameter space is found in Fig. 2; the parameters for each run are included in Table 1. The variation of length of the estuary with mixing rate is clearly evident. The length also varies with river flow, but not as dramatically. All of the solutions are stratified, and the highest stratification is observed for the highest river flow. A hydraulic control is maintained at the mouth in all cases, with a sharp rise in the isohalines and localized internal waves at the transition.

Although these runs encompass a broad range of parameter space and the length of the estuary varies by almost two orders of magnitude, the lower-layer velocity (see the appendix for definition) is remarkably uniform (see Table 1), varying from 0.09 m s^{-1} for the most weakly forced case to 0.17 m s^{-1} for the most strongly forced case. This result indicates the robustness of the estuarine circulation and its relative insensitivity to forcing variations.

The spatial structure of the salinity and velocity fields for several cases is shown in Fig. 3. The case shown in the left panel shows moderate river flow and weak mix-

ing, resulting in a relatively long salinity intrusion with a classic, partially mixed structure. The composite Froude number is almost constant, at a value of close to 0.5, through the entire estuary until near the mouth, where it increases to slightly over one past the control point. The case shown in the center panel has the same river flow, but twice as much mixing. The solution is nearly identical except that the length has shortened by a factor of 2. The case shown in the right panel indicates how high river flow results in a salt wedge regime, with most of the salinity gradient confined to the lower layer.

Figure 4 shows a detailed comparison of analytical function dependencies versus those in the numerical model. All of the variables show a qualitative agreement with the analytic scaling laws, with minor differences in parts of parameter space. The length of the estuary varies linearly with mixing rate, and both stratification and estuarine velocity are almost invariant with mixing, as predicted by theory. The length of the estuary shows the predicted $u_f^{-1/3}$ behavior except for high river flows where the length scale varies more sensitively. The estuary is more like a salt wedge at high freshwater flow

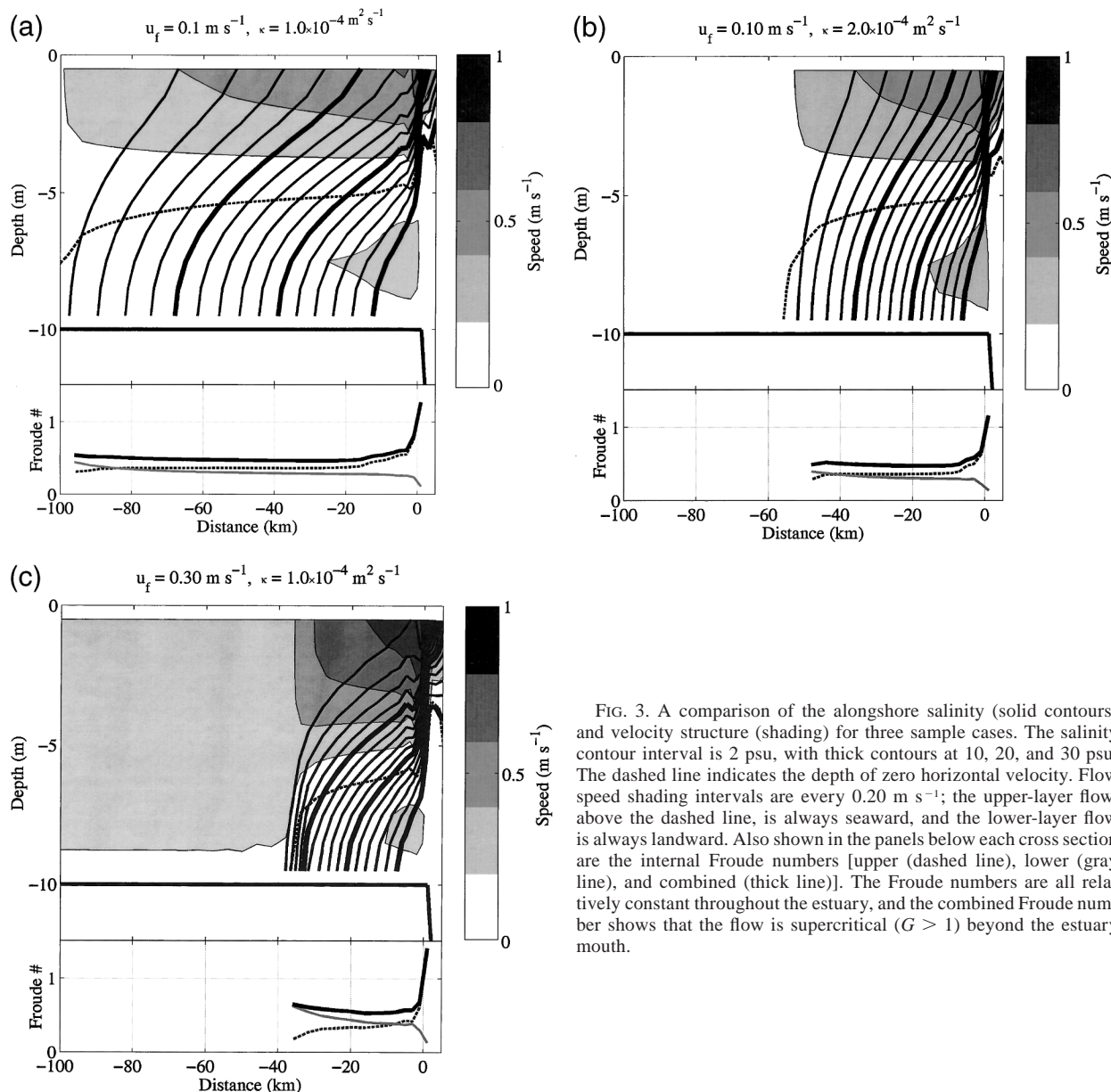


FIG. 3. A comparison of the alongshore salinity (solid contours) and velocity structure (shading) for three sample cases. The salinity contour interval is 2 psu, with thick contours at 10, 20, and 30 psu. The dashed line indicates the depth of zero horizontal velocity. Flow speed shading intervals are every 0.20 m s⁻¹; the upper-layer flow, above the dashed line, is always seaward, and the lower-layer flow is always landward. Also shown in the panels below each cross section are the internal Froude numbers [upper (dashed line), lower (gray line), and combined (thick line)]. The Froude numbers are all relatively constant throughout the estuary, and the combined Froude number shows that the flow is supercritical ($G > 1$) beyond the estuary mouth.

rates, and the assumptions leading to the length-scale dependence on $u_f^{-1/3}$ are significantly violated as the river flow velocity, u_f , approaches the estuarine velocity. The dependence of stratification on river flow shows that the $u_f^{2/3}$ relationship is consistent with theory, except for the high-river-flow cases, again because the scaling assumptions are violated in the salt wedge regime when Δs approaches s_0 (here 25 psu, the bottom salinity that defines the point where the stratification is measured). The estuarine velocities show the theoretically predicted $u_f^{1/3}$ dependence throughout parameter space.

Monismith et al. (2002) notes that the estuarine length scale may vary by less than $u_f^{1/3}$ if mixing and stratification are coupled; in fact, they found a length-scale

dependence of $u_f^{1/7}$. In this very idealized study, mixing is specified as constant throughout the estuary and has no dependence on stratification. Therefore, the length scale is expected to have a $u_f^{1/3}$ dependence.

In addition to confirming the analytical scalings discussed in section 2a, the numerical results also show that the dominant balances of salt and momentum assumed in the derivation of those scaling are mostly correct. But again, there are some important points of derivation. Numerical results show that the horizontal salt flux is indeed primarily balanced by vertical salt diffusion for all cases except those with high freshwater flows. Calculations of integrated salt flux show that contributions due to vertical salt advection are only 20%

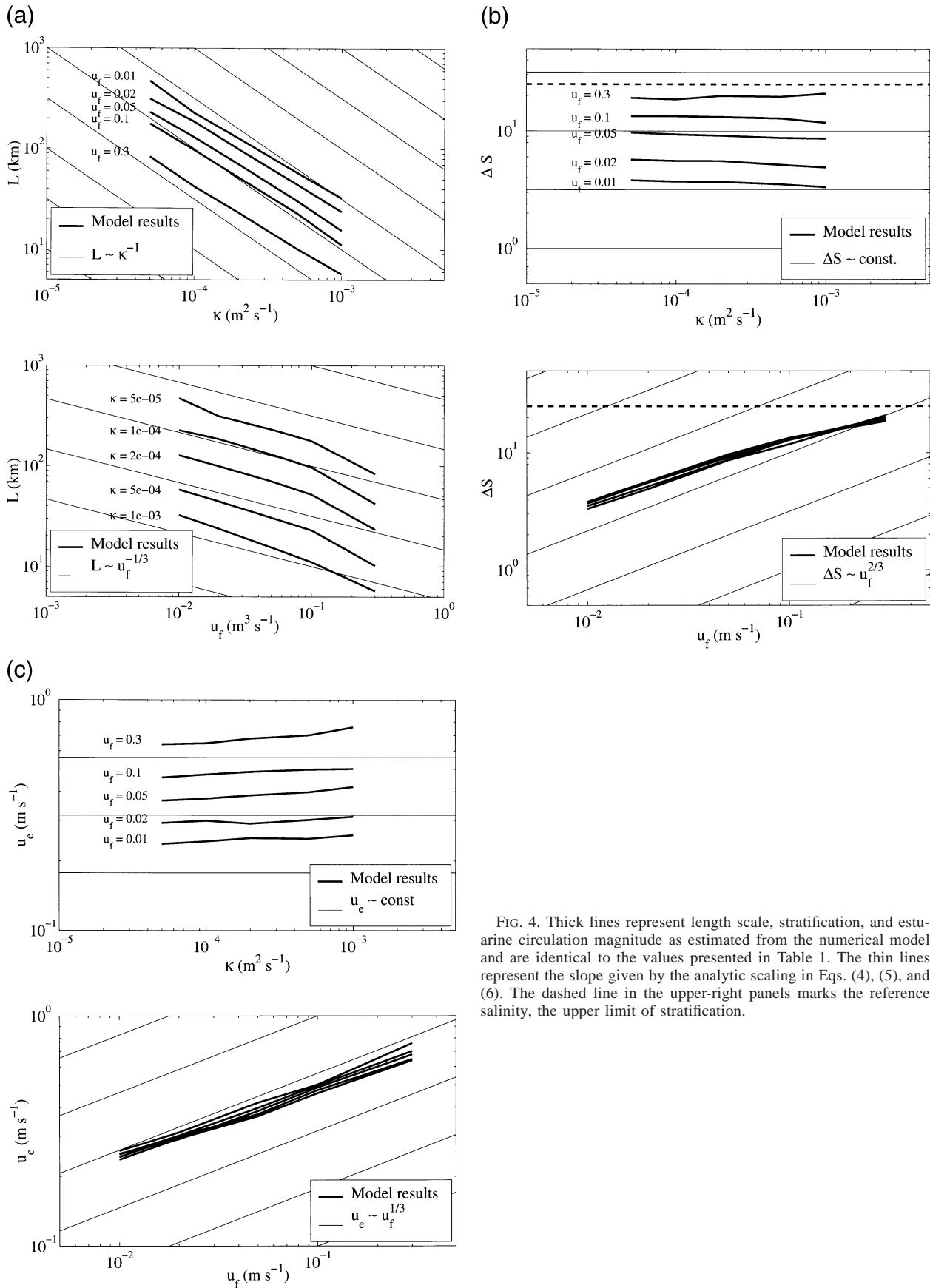


FIG. 4. Thick lines represent length scale, stratification, and estuarine circulation magnitude as estimated from the numerical model and are identical to the values presented in Table 1. The thin lines represent the slope given by the analytic scaling in Eqs. (4), (5), and (6). The dashed line in the upper-right panels marks the reference salinity, the upper limit of stratification.

TABLE 2. The adjustment time scale τ_u of estuarine response to a shift in freshwater flux estimated for the six cases shown using the parameters on the left (see text for details). Also listed is the speedup factor α_u , relating the actual adjustment time scale τ_u to the advective time scale τ_f .

u_{f1} (m s ⁻¹)	u_{f2} (m s ⁻¹)	κ ($\times 10^4$) (m ² s ⁻¹)	L_1 (km)	L_2 (km)	τ_f (days)	τ_u (days)	α_u
0.1	0.02	1	85	179	76	15.0	1.70
0.1	0.02	2	45	95	41	12.3	1.10
0.1	0.02	5	19	42	18	7.1	0.82
0.02	0.1	1	179	85	15	6.1	4.19
0.02	0.1	2	95	45	8.1	3.5	3.91
0.02	0.1	5	42	19	3.5	1.4	4.28

to 30% as strong as vertical salt diffusion for all but the high flow cases, where the contributions are approximately equal. The numerical results also confirm that the dominant balance in the longitudinal momentum equation is between vertical viscosity and the horizontal pressure gradient.

The theoretical scaling is based on the assumption that the longitudinal salt gradients are constant with respect to depth at a given point in the estuary. This is clearly not true for high discharge flows in which the upper layer is very fresh, with nearly no horizontal salt gradient. However, the assumption is violated even in parts of parameter space that have good agreement with the linear scaling, indicating that the solution is not sensitive to vertical variations in the longitudinal salinity gradient.

5. Time-dependent results

The steady-state results discussed in the previous section show some characteristics inconsistent with observations. For example, the often observed variation of stratification with vertical mixing (e.g., Hass 1977; Jay and Smith 1990) does not occur. In addition, there is no point in the examined parameter space where the modeled estuary is well mixed, whereas there are many such examples in nature. The later discrepancy may be related to the neglect of horizontal tidal dispersion. However, we find that these common features of estuarine observations are produced when time-dependent mixing is introduced in the model. Before considering time-dependent mixing, however, it is instructive to consider the time scale of response to changes in river flow.

a. Step change in freshwater flux

The response of an estuary to a step change in freshwater forcing is estimated numerically by running simulations, identical to those described in the previous section, to steady state, and then either increasing or decreasing the freshwater discharge to a new constant value. An actual step in the freshwater discharge is not possible because of spurious waves excited by the discontinuity, so a continuous approximation is used:

$$Q(t) = \frac{1}{2}(U_{f2} - U_{f1}) \tanh[2(t - t_0)] + \frac{1}{2}(U_{f1} + U_{f2}), \tag{10}$$

where U_{f1} and U_{f2} are the respective initial and final freshwater flow speeds, t is the time (in days), and t_0 the time of change in discharge. Using this formulation, the switch in freshwater discharge occurs over approximately two days, which will be shown to be shorter than the adjustment time scale for all the cases investigated.

Six cases are evaluated (listed in Table 2), three with increasing discharge and three with decreasing discharge. The adjustment time scale is estimated by using a least squares fit to exponential decay of the initial length scale toward the final length scale (Fig. 5). The length scale is defined by the average value of $\partial s/\partial x$ between 5 and 25 psu.

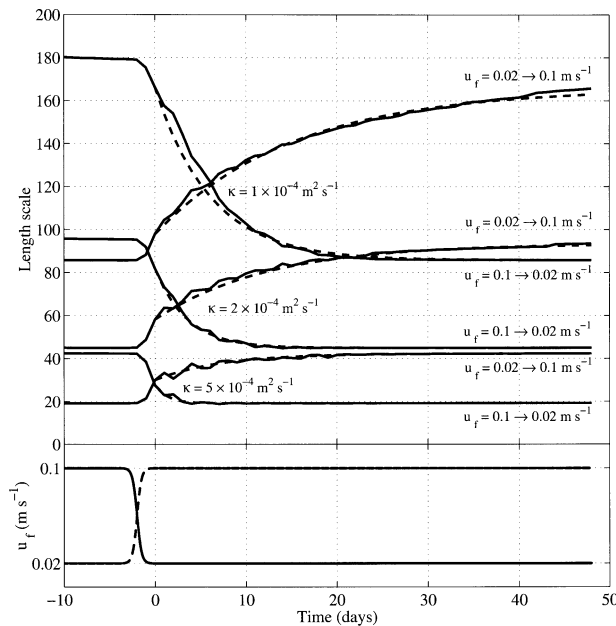


FIG. 5. Estuarine length scales shown as a function of time for the parameters used in Table 2. The time axis is shifted such that the fit to exponential decay (to estimate the time scale of adjustment) begins at $t = 0$, two days after t_0 , the midpoint in freshwater flux change [see Eq. (10)]. The slight lag between the step in u_f and $t = 0$ is included to ensure that the estuary is responding to the freshwater flux and results in better fits than using a smaller lag. The fitted functions are shown by dashed lines. The lower panel shows the two freshwater flux cases as a function of time.

As expected, longer adjustment times correspond to longer salinity intrusion length. However, there was a surprisingly large difference in adjustment times depending on whether the freshwater flow was increasing or decreasing. The longest estuary case adjusted to the new flow conditions over two times faster for an increase in flow as compared to a decrease, and the shorter estuaries showed an even greater asymmetry in response. This asymmetry is inconsistent with the linear theory of Kranenburg (1986).

The asymmetric response to forcing seems to be explained by the nonlinear effects of bottom drag. In cases with decreasing flow, the motion of the salt wedge adds constructively to the lower layer flow, resulting in an increase in bottom drag. For increasing freshwater flux, the estuary shortens so that the depth average motion of the salt intrusion is seaward, opposing the landward flow in the lower layer. This causes the net bottom velocity to be smaller, resulting in a smaller bottom drag. The increased drag increases the adjustment time scale.

The values of α_u [Eq. (8)] were estimated by comparing the estimated adjustment time scale, τ_u , derived from the numerical to the advective time scale defined using the average of the freshwater flow rates and end-member steady-state length scales. Although Kranenburg (1986) predicts a value of $\alpha_u = 6$, the estimates for α_u , listed in Table 2, were uniformly smaller than 6; the estimated adjustment time scale is always slower than predicted for a prismatic estuary.

For an estuary to adjust at the rate predicted by Eq. (7), at the instant of the change in freshwater flow all of the additional freshwater flux, ΔQ_f , must remain within the estuary and be used to modify the estuarine salt structure. This additional freshwater changes the total freshwater content of the estuary, primarily through changes in the salinity intrusion length scale. This process continues until it has reached its new steady state. The numerically simulated estuaries did not convert all of the additional freshwater flux into changes in salinity structure, slowing the adjustment time scale proportionally. The reasoning is similar for a decrease in river discharge, where the negative freshwater anomaly of the decreasing discharge must correspondingly reduce the freshwater contained in the estuary.

b. Spring/neap modulation of vertical mixing

The basic numerical model configuration was modified such that the (spatially constant) vertical mixing within the estuary is modulated with a fortnightly period, from $\kappa = 1.0 \times 10^{-4}$ to $5.0 \times 10^{-4} \text{ m}^2 \text{ s}^{-1}$. Constant values of river discharge with $u_f = 0.01, 0.05$, and 0.10 m s^{-1} are used in the three consecutive runs described below.

Vertical profiles are shown in Fig. 6 for three river discharges. In contrast with the steady-state runs, shown in the previous section, the spring/neap runs show that varying diffusivity/viscosity can modify the stratifica-

tion as well as producing well-mixed conditions for low river flow. Changes in stratification are more pronounced for the high-flow cases because the maximum stratification is greater for higher flows, but all cases indicate significant changes.

Cross sections for the three cases (Fig. 7) indicate that there are only small variations in the length of the estuary through the spring–neap cycle for the low discharge case, and increasing changes in length for larger river flows. This is consistent with the faster response of the estuary to changes in forcing at higher flows. The absence of significant changes in estuarine length during low discharge explains why there are large changes in stratification on the spring–neap time scale, as indicated in Eq. (2). Without a commensurate adjustment in the salinity gradient, changes in mixing will result in quadratic changes in stratification.

Again, the adjustment time scale will be compared to the advective time scale, $\bar{\tau}_f = \bar{L}/u_f$, here defined by the mean length scale of the estuary, \bar{L} . The speedup factor α_κ , which relates the adjustment time scale of the estuary due to changes in vertical mixing to the freshwater advective time scale $\bar{\tau}_f$, is defined as

$$\alpha_\kappa = \frac{\bar{\tau}_f}{\tau_\kappa} = \frac{1}{\tau_\kappa} \frac{\bar{L}}{u_f}. \quad (11)$$

The oscillatory forcing frequency ω_f may be used to estimate the deviation from the mean length scale ΔL for a particular forcing frequency. We assume that the estuary response is similar to a damped system with oscillatory forcing so that ΔL roughly follows

$$\tau_\kappa \frac{d\Delta L}{dt} + \Delta L = \Delta L_{\max} \sin(\omega_f t), \quad (12)$$

where τ_κ is the adjustment time scale of the estuary to step changes in vertical mixing, the damping time scale of the unforced solution, and $\Delta L_{\max} \equiv \frac{1}{2}[L(\kappa_{\min}) - L(\kappa_{\max})]$ is the maximum length scale excursion based on the range of the mixing coefficient. Taking only the nondecaying part of the ΔL solution, the complete equation for the estuarine length scale becomes

$$L = \bar{L} + \frac{\Delta L_{\max}}{1 + (\omega_f \tau_\kappa)^2} [\sin(\omega_f t) - \omega_f \tau_\kappa \cos(\omega_f t)]. \quad (13)$$

If the forcing time scale is much larger than the adjustment time scale ($\omega_f \tau_\kappa \ll 1$), the estuary will keep up with the forcing, and the solution will span the entire range of length scales available for the given range in mixing. The solution will be in phase with the forcing, with the largest estuarine length scales occurring at exactly the time of lowest mixing. On the other hand, if the adjustment time scale is short with respect to the forcing time scale ($\omega_f \tau_\kappa \gg 1$), the estuarine length scale will respond very little to the changes in mixing, with $\Delta L \ll \Delta L_{\max}$. In this case, the response will be out of phase with the mixing, with the maximum estuarine length scale lagging the time of the lowest mixing by

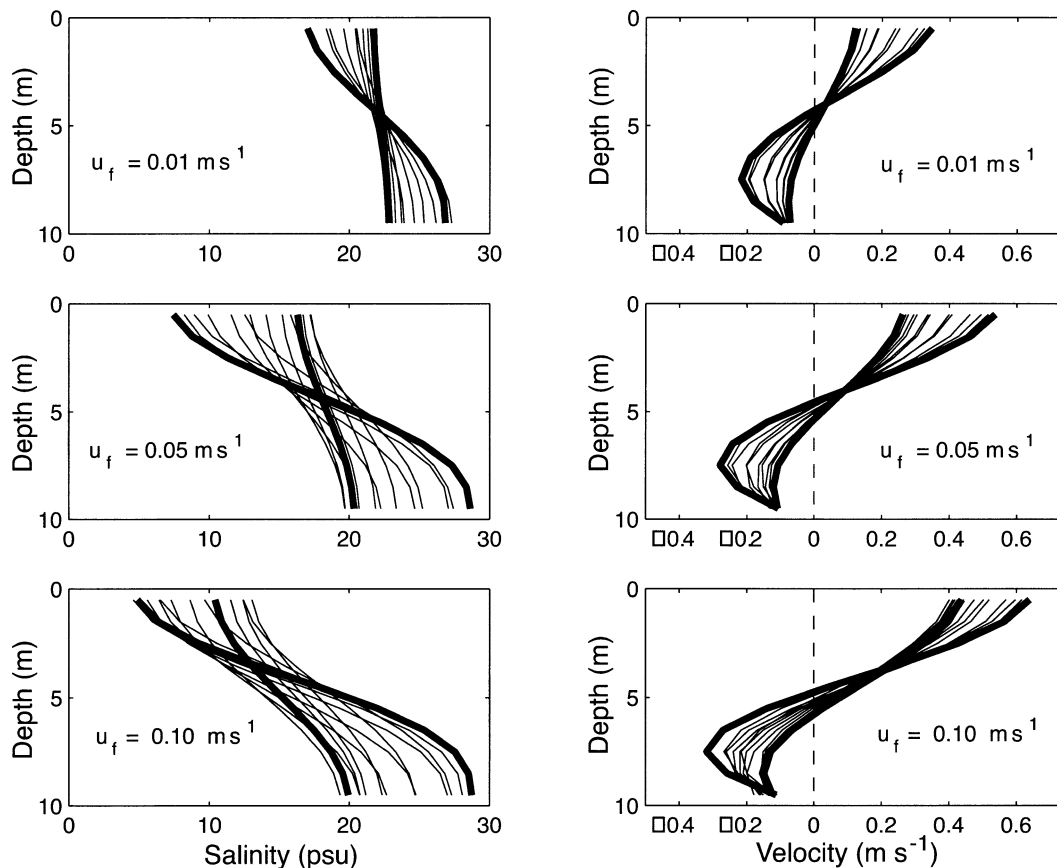


FIG. 6. Spring/neap variations in velocity and stratification are shown for the three riverine discharge cases also shown in Fig. 7. The boldface lines represent the positions of the profiles during maximum spring and neap (spring profiles have lower vertical gradients in all cases). The profiles were taken at the point in the estuary where the mean bottom salinity was 25 psu.

up to 90° . The phase lag predicted from Eq. (13) is consistent with model results, 2–3 days for the parameters used here.

Figure 8 shows the time-dependent changes in estuarine length scale in relation to the steady-state end-member length scales for the $u_f = 0.10$ and 0.01 m s^{-1} cases from Fig. 6. Bars representing the predicted amplitude in estuarine length scale are shown for $\alpha_\kappa = 2$ and 6 for each case, using Eq. (11) to calculate τ_κ . The response of the length scale to mixing is not symmetric. The instantaneous adjustment time scale increases as the estuary length increases, so it may be misleading to try to estimate α_κ , or equivalently τ_κ , from the numerical results. However, it is clear from Fig. 8 that for the longer estuary ($u_f = 0.10 \text{ m s}^{-1}$) $\alpha_\kappa \sim 2$, where for the shorter estuary $\alpha_\kappa \sim 6$.

6. Relation to Stommel and Farmer's "overmixed" estuary

Comparisons between the overmixing theory, described in section 2, and the numerical solution show that the modeled estuary is not overmixed. The ex-

change flow at the mouth is always submaximal, as the upper-layer thickness is never more than half of the total water depth. Even though the exchange at the mouth is not maximal, the properties of the estuarine exchange still follow the same parameter dependence as that predicted by overmixing theory. Stratification and exchange at the mouth predicted by the numerical model are consistently about 70% of the limits predicted by overmixing theory (shown in Fig. 9). Only for very strong freshwater discharge does the normalized numerical stratification increase slightly, as might be expected for a solution that resembles a salt wedge.

The numerical solution has the same dependence on mixing and river discharge as that predicted by overmixing theory. In an overmixed estuary, stratification and exchange at the estuary mouth depend only on freshwater discharge and estuarine geometry at the mouth; the *intensity* of mixing (the magnitude of κ) does not affect the *amount* of mixing (the vertical salt flux). This result is identical to the steady-state solutions of Hansen and Rattray (1965) and Chatwin (1976), discussed in section 2, and demonstrated numerically in section 4. These solutions also predict that the estuarine

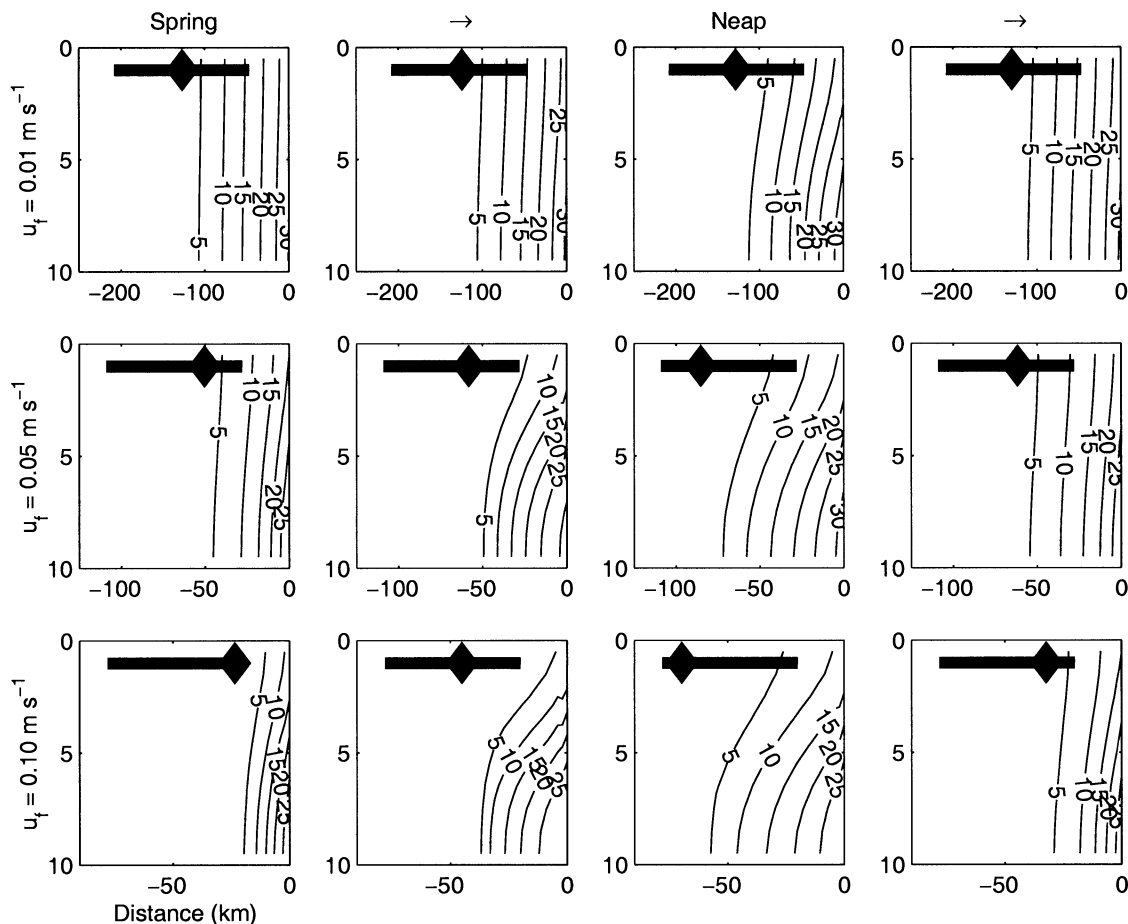


FIG. 7. Spring/neap cross sections of salinity are contoured for various values of riverine discharge. Snapshots of salinity structure are shown at four times in the spring/neap cycle, so the progression of time is to the right and is cyclic. The boldface line at the top of each panel represents the range of estuarine lengths estimated by the steady-state end members calculated from the riverine discharge u_f and the minimum and maximum diffusivity/viscosity κ [$L(\kappa_{\min})$ $L(\kappa_{\max})$]. The sliding diamond marker on the bar represents the instantaneous length scale calculated from the salinity structure at that particular time. The frames shown are not in phase with the forcing, but are lagged by 2 days so that the maximum and minimum extent of the estuary is displayed (see Fig. 8).

stratification is independent of the vertical eddy diffusivity/viscosity, κ (see Fig. 4). Thus, in both an estuary with exchange critically controlled at a constriction and an estuary that has a structure controlled by internal dynamics, steady-state stratification is not affected by increasing turbulence.

7. Discussion

The idealized regime used in this paper for the setup of the numerical simulations was chosen because it affords direct comparisons with theoretical results. Although there are clear advantages to this approach, there are a number of important processes that were not considered because of the simplifying assumptions made from the outset. Here we speculate on the consequences of ignoring some of these potentially important processes, and limitations of the results presented above.

One important limitation is the decoupling of mixing

and stratification. The numerical simulations all used spatially constant mixing. Other simulations, not presented, used a stratification-dependent mixing closure. These simulations tended toward runaway stratification because the mixing in the pycnocline, where stratification was strong, was reduced to background levels, that is, the preset minimum value for mixing in the closure scheme used.¹ This runaway stratification is in part a consequence of the simplicity of the spatial domain; the inclusion of sloping sidewalls or bathymetric variations can prevent runaway conditions (e.g., MacCready et al. 2002).

In this paper, as in Hansen and Rattray (1965) and

¹ All modern mixing closures, for example, both Mellor and Yamada (1974) and Large et al. (1994), use some minimum mixing value, specified as one of the tunable parameters in the algorithm. This value is supposed to represent the background, or molecular mixing, that is thought to occur throughout the domain.

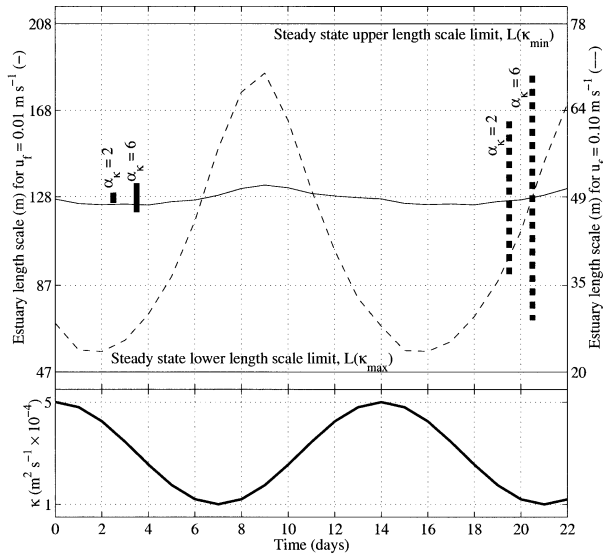


FIG. 8. Spring/neap variations in length scale are shown for the low-flow case ($100 \text{ m}^3 \text{ s}^{-1}$) with a solid line using the left-hand scale, and the high-flow case ($1000 \text{ m}^3 \text{ s}^{-1}$) with a dashed line using the right-hand scale. Both the left- and right-hand axes are normalized such that $L(\kappa_{\min})$ and $L(\kappa_{\max})$ each overlap on the graph. The estuarine length scale for the low-flow case covers a much smaller percent of the available range, based on $L(\kappa_{\min})$ and $L(\kappa_{\max})$, when compared with the high-flow case that spans most of the available range. The thick vertical lines represent the length-scale deviations estimated from Eq. (13). The lower panel shows the phase of the vertical mixing. Length scales are shortest during high mixing and longest during low mixing, as expected, with a phase lag of 2–3 days.

Chatwin (1976), vertical mixing is treated as an independent parameter, proportional to tidal magnitude. Monismith et al. (2002) show that, in the presence of tides, vertical mixing depends on the river discharge, and hypothesized that this was the cause of an observed relationship between estuarine length scale, $L \sim u_r^{-1/7}$, much weaker than that suggested by tidally averaged theory.

8. Conclusions

A numerical model has been used to confirm scaling relations based on Hansen and Rattray (1965) and Chatwin (1976). These scaling relations are based on several assumptions: first, that the salt flux is dominated by the estuarine circulation; second, that the estuarine circulation is significantly stronger than the river flow; third, that the estuary lies within a rectangular, prismatic channel. These assumptions limit the general application of the results to real estuaries; however, they allow direct comparison with theory.

Numerical results show that an idealized estuary configuration with constant vertical mixing within the estuary behaves as predicted by classical theories of estuarine circulation. Estuarine scales estimated from the numerical solutions have the same functional depen-

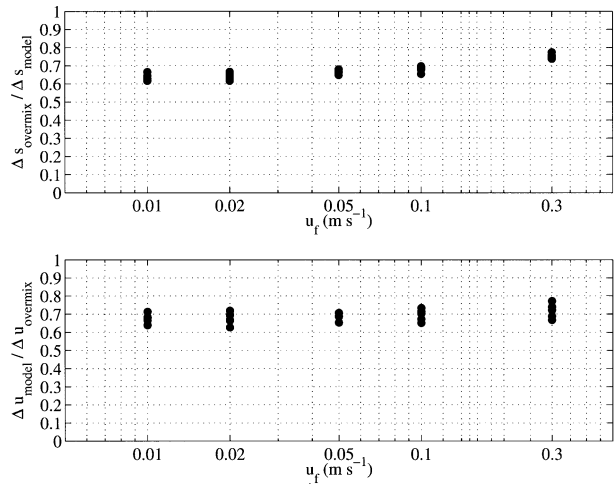


FIG. 9. (top) Numerically predicted stratification and (bottom) exchange flow are plotted as a function of the freshwater flow speed u_f . Because stratification is smallest for an overmixed estuary, the inverse of the normalized salinity has been plotted. Numerical values were calculated at the mouth. The reference salinity used for the overmixing calculations was the inflowing lower-layer-averaged salinity, using the method described in the appendix.

dencies as the analytical solutions derived by Hansen and Rattray (1965) and Chatwin (1976):

$$L \sim \kappa^{-1} u_f^{-1/3}, \tag{14}$$

$$u_e \sim u_f^{1/3}, \text{ and} \tag{15}$$

$$\Delta s \sim u_f^{2/3}. \tag{16}$$

Vertical stratification, Δs , predicted by the model is closely related to that predicted for an overmixed estuary described by Stommel and Farmer (1953), although the numerical solutions are not overmixed. These results demonstrate that estuarine stratification and exchange are independent of the magnitude of turbulent mixing and depend only on the estuarine geometry and the magnitude of freshwater discharge, given the assumptions listed above.

Simulations with time-dependent forcing showed that estuarine time scales of adjustment were between 1 and 6 times the freshwater advective time scale, L/u_f , for both step changes in freshwater discharge and oscillatory changes in the intensity of turbulence. Estuaries with very long adjustment time scales will respond little to the quick periodic forcing. In this case, the estuarine length scale will remain near the mean of the steady-state end-member length scales, the steady-state length scale that the estuary would have under the minimum and maximum values of vertical mixing. The time-dependent estuarine length scale will closely track the steady-state length scale when the adjustment time scale is on the order of or less than the period of the forcing; however, the estuary may still not be in a quasi steady balance in terms of stratification and estuarine circulation. Time dependence is thus an essential consider-

ation if stratification varies with the magnitude of turbulent mixing.

Acknowledgments. The authors thank Parker MacCready for many helpful comments on numerous early drafts of this paper. This work was supported by the Office of Naval Research, Processes and Prediction Division, Award N00014-01-1-0199.

APPENDIX

Definitions

a. Definition of terms

H	Estuary depth
W	Estuary width
g	Gravitational acceleration constant (9.8 m s^{-2})
β	Parameter relating salinity to density ($\rho = \rho_0 + \beta s$)
s_0	Reference salinity
$f_n(z)$	Order-one polynomial in z
u_f	Depth average estuarine flow, equal to the average freshwater flow
Q_f	Freshwater transport ($Q_f = HWu_f$)
ν	Vertical viscosity
K_z	Vertical diffusivity
κ	Generalized vertical mixing ($\kappa = \nu = K_z$)
u	Along-channel estuarine flow velocity
u_e	Estuarine exchange flow ($u_e = u - u_f$)
$u_{1,2}$	Upper (1) and lower (2) layer velocity.
Δu	Velocity difference between upper and lower layer ($\Delta u = u_2 - u_1$)
s	Salinity
Δs	Salinity difference between upper and lower layer ($\Delta s = s_2 - s_1$)
$s_{1,2}$	Upper (1) and lower (2) layer salinity.
L	Estuarine length scale ($L \sim s_0/s_x$)
τ_f	Advective time scale (u_f/L)
τ_u	Estuary adjustment time scale in response to changes in freshwater discharge
τ_κ	Estuary adjustment time scale in response to changes in vertical mixing
α_u	Speedup factor defined by the ratio τ_u/τ_f
α_κ	Speedup factor defined by the ratio τ_κ/τ_f

b. Calculation of estuarine scales

The scale estimates from the numerical model are also presented numerically in Table 1, which lists various estuarine characteristics over the parameter space of the numerical model runs. Here the methods used for calculating these scales are described.

Length scale was estimated by first calculating the average longitudinal bottom salinity gradient between 5 and 25 psu. Then, the length scale was calculated as the hypothetical distance between freshwater and oceanic water (32 psu), assuming this spatial gradient.

Calculations of the stratification are weighted by salt flux so that, for example, the “upper layer” salinity is given by

$$s_1 = \frac{\int_{-h}^0 su \, dz}{\int_{-h}^0 u \, dz}, \quad (\text{A1})$$

where $z = -h$ is the point where $u = 0$, the interface between the upper and lower layers. Layer velocity is calculated as the average velocity in each layer. The calculations are made at the point in the estuary where the bottom salinity was 25 psu, which maintained a constant position relative to the estuary, although the point moved relative to the topography. In this way, the calculations are done at the same point in the estuary relative to the estuary itself, despite order-one changes in estuarine length. The vertical stratification Δs is calculated as the difference between the upper and lower layers, where the lower layer is fresher than 25 psu because of the averaging in the layer.

REFERENCES

- Abood, K. A., 1974: Circulation in the Hudson Estuary. *Ann. N. Y. Acad. Sci.*, **250**, 39–111.
- Armi, L., and D. M. Farmer, 1986: Maximal two-layer exchange through a contraction with barotropic net flow. *J. Fluid Mech.*, **164**, 27–51.
- Chatwin, P. C., 1976: Some remarks on the maintenance of the salinity distribution in estuaries. *Estuarine Coastal Mar. Sci.*, **4**, 555–566.
- Fong, D. A., 1998: Dynamics of freshwater plumes: Observations and numerical modeling of the wind-forced response and along-shore freshwater transport. Ph.D. thesis, Joint Program in Oceanography, MIT/WHOI, 173 pp.
- Haidvogel, D. B., H. Arango, K. Hedstrom, A. Beckmann, P. Malanotte-Rizzoli, and A. Shchepetkin, 2000: Model evaluation experiments in the North Atlantic basin: Simulations in nonlinear terrain-following coordinates. *Dyn. Atmos. Oceans*, **32**, 239–281.
- Hansen, D. V., and M. Rattray, 1965: Gravitational circulation in straits and estuaries. *J. Mar. Res.*, **23**, 104–122.
- , and —, 1966: New dimensions in estuary classification. *Limnol. Oceanogr.*, **11**, 319–326.
- Hass, L. W., 1977: The effect of the spring–neap tidal cycle on the vertical structure of the James, York and Rappahannock Rivers, Virginia, U.S.A. *Estuarine Coastal Mar. Sci.*, **5**, 485–496.
- Hunkins, K., 1981: Salt dispersion in the Hudson Estuary. *J. Phys. Oceanogr.*, **11**, 729–738.
- Jay, D. A., and J. D. Smith, 1990: Circulation, density distribution and neap–spring transitions in the Columbia River estuary. *Mixing in Estuaries and Coastal Seas*, C. Pattiaratchi, Ed., Amer. Geophys. Union, 211–249.
- Kranenburg, C., 1986: A time scale for long-term salt intrusion in well-mixed estuaries. *J. Phys. Oceanogr.*, **16**, 1329–1331.
- Large, W. G., J. C. McWilliams, and S. C. Doney, 1994: Oceanic vertical mixing: A review and a model with a nonlocal boundary layer parameterization. *Rev. Geophys.*, **32**, 363–403.
- Linden, P. F., and J. E. Simpson, 1988: Modulated mixing and frontogenesis in shallow seas and estuaries. *Cont. Shelf Res.*, **8**, 1107–1127.

- MacCready, P., 1999: Estuarine adjustment to changes in river flow and tidal mixing. *J. Phys. Oceanogr.*, **29**, 708–729.
- , R. D. Hetland, and W. R. Geyer, 2002: Long-term isohaline salt balance in an estuary. *Cont. Shelf Res.*, **22**, 1591–1601.
- Mellor, G. L., and T. Yamada, 1974: A hierarchy of turbulent closure models for planetary boundary layers. *J. Atmos. Sci.*, **31**, 1791–1806.
- Monismith, S. G., W. Kimmerer, J. R. Burau, and M. T. Stacey, 2002: Structure and flow-induced variability of the subtidal salinity field in northern San Francisco Bay. *J. Phys. Oceanogr.*, **32**, 3003–3019.
- Nof, D., and T. Pichevin, 2001: The ballooning of outflows. *J. Phys. Oceanogr.*, **31**, 3045–3058.
- Pritchard, D. W., 1952: Salinity distribution and circulation in the Chesapeake Bay estuarine system. *J. Mar. Res.*, **15**, 33–42.
- , 1954: A study of the salt balance in a coastal plain estuary. *J. Mar. Res.*, **13**, 133–144.
- Stommel, H., and H. G. Farmer, 1953: Control of salinity in an estuary by a transition. *J. Mar. Res.*, **12**, 13–20.
- Yankovsky, A. E., and D. C. Chapman, 1997: A simple theory for the fate of buoyant coastal discharges. *J. Phys. Oceanogr.*, **27**, 1386–1401.